The Journal of National Chiao Tung University
Vol. I, April 1976
pp. 103-122

銻化銦之準靜態變動特性

Quasi-Static Transport Characteristics of Indium Antimonide

蔡 中 Chun Tsai
Department of Electronics Engineering

(Received December 31, 1976)

ABSTRACT — The I-V characteristics of over 150 bulk InSb single crystals at 78°K have been measured. These samples, 1mm x 1mm in cross section and 0.4 to 13mm in length, are of either the p- or n-type with carrier concentration ranging from 2.5×10^{13} to 2.1×10^{16} /cm^3. These multi-valued I-V characteristics were found to be highly non-linear, with as much as four distinct regions each of which can be attributed to a different transport mechanism. Furthermore, these characteristics were found to be dependent not only on the carrier type and doping density of the sample but also on the contact material (In or Sn) used. A theoretical explanation of the observed behavior will be presented.

I. Introduction

Although high frequency generation in the range from a few MHz [1-2] to some 100 GHz [3-4] in InSb has been reported by a number of investigators [5-6] a totally satisfactory explanation of the associated phenomena has yet to be formulated [7]. As to the investigation of the static properties of InSb in the absence of a magnetic field, very little has been reported; Eastman [8] has performed some static experiments with a sample 3 mils in length. In order to better understand the transport mechanisms in InSb, we undertook an extensive investigation of its quasi-static properties. Brief reports of our investigation have been presented previously [9-10].

The I-V characteristics of 158 bulk InSb single crystals, 1mm x 1mm in cross section and 0.4 to 13mm in length, with n or p-type carrier densities ranging from 2.5×10^{13} to 2.1×10^{16}/cm^3, have been measured at 78°K. For some combination of doping, carrier type,

and contact material, the current first increases linearly, then saturates as the voltage is increased. For still higher applied voltages, the current increases rapidly giving rise to a negative differential resistance (NDR). For other cases, current first increases nonlinearly with voltage and then pass directly into the NDR region. Current saturation can be explained by intra-valley scattering while the negative resistance is attributed to an avalanche phenomenon. When a pulse source voltage and a magnetic field is applied to the sample, large amplitude current oscillations in the 30 Mc/sec region can occur [9-10].

For multi-valued I-V characteristics such as those associated with InSb the shape of the observed curve is dependent upon the value of external resistance. This phenomenon can be understood by referring to Fig. 1 which is a representative sketch of the true and the observed I-V characteristic of a class of InSb samples at a given external resistance. The positive directions for I and V in the figure have been chosen for easy comparison with experimental curves obtained using a transistor curve tracer to be presented later.

In Fig. 1, the true I-V characteristic is sketched as a solid curve. For a given value of the external resistance R_e, the observed I-V curve is indicated by a dotted curve wherever it departs from the true curve. Starting from a zero source voltage (corresponding to the initial point at the origin, $V_d=I=0$), the current I and the sample voltage V_d both increase as the source voltage V_s is increased until point A is reached. At this point, values of I and V_d corresponding to those at point A changes to those corresponding to point A' with no additional increase in V_s. The straight line segment A-A' simply corresponds to the load line whose equation is:

$$I=\frac{V_{sA}-V_d}{R_e}$$

where V_{sA} is the source voltage corresponding to point A. In other words, the slope of the load line is given by $-1/R_e$. Thus, if the true curve at point A is truly discontinuous, an R_e approaching zero in value will be required in order for the observed curve to faithfully follow the true one. From A' to B the current I is constant as V_s is increased and the observed and true curves coincide. With

no further increase in V_s at B, the values of I and V_d jump from those corresponding to point B to those corresponding to point B' In other words from B to B', the observed line segment, whose slope is given by $-1/R_e$, again departs from the true curve. For the observed and true curves to coincide here it would be necessary to increase R_e until $-1/R_e$ is equal to slope of the upper branch of the curve at point B. If V_s is increased further, the observed and true curves, with increasing I, again coincide.

Now, if V_s is decreased, the observed and true curves remain coincident until point G is reached at which point a jump from G to G' following the load line again occurs. To faithfully follow the true curve from G to B, it would also be necessary to increase R_e until $1/R_e$ is equal to the slope of the upper branch of the curve at point B. If V_s is decreased still further, I remains constant until point H is reached at which point a jump from H to H' following the load line again occurs. If the discontinuous segment of the curve H-A were to be observed, we see that a zero R_e is required. As V_s is reduced to zero, the observed and true curves again coincide, from point H' to the origin.

To summarize, it is necessary to change the value of R_e during the course of measurement if the entire true curve were to be observed. This procedure was followed in all the measurements reported here. It must be emphasized, however, that since Fig. 1 is a plot of the current through the sample v.s. the voltage across it, all portions of the observed characteristic regardless of the value of R_e, except for the load lines between discontinuities, constitute true, though incomplete, representations of the I-V relationship of the smaple.

II. Experimental Results

1. Specimen

Six kinds of indium antimonide samples were used in our experiments. They were all single crystals, but were different in type and degree of doping, designated by the abbreviated terms PH, PM, PL, NH, NM, and NL. The first letter, P or N, indicates the type of doping. The second letter, H, M or L, stands respectively for relatively high, medium, or low level of doping concentration. A total of 158 samples were cut from six ingots in the form of bars approximately 1mm x 1mm in cross-section and with lengths varying

from less than a millimeter to more than ten millimeters in the [211] direction.

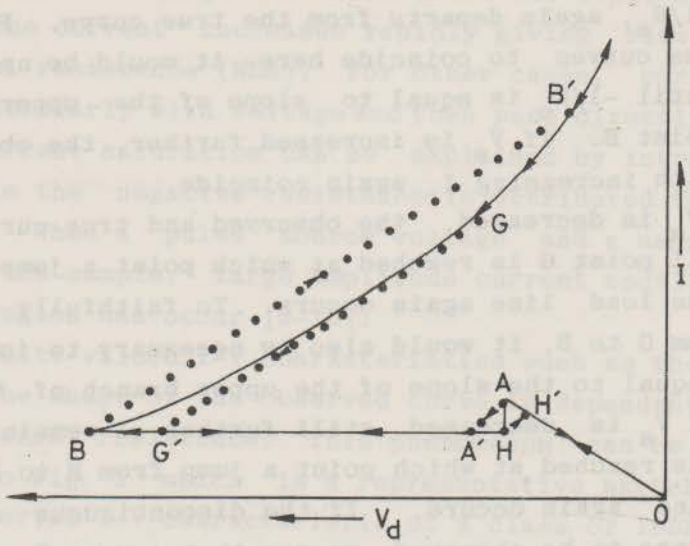

Fig. 1. True and observed I-V characteristics showing influence of external resistance.

The samples were subjected to a chemical treatment after they were cut from an ingot to remove the attached abrasive material during cutting. First the samples were soaked in deionized water for a short while and then bathed in acetone for a couple of seconds and then the procedure was repeated two more times. Just before a sample was soldered and mounted on a coaxial cable, both of its ends were etched in CP-4 solution for a short time, then rinsed with deionized water and dried with nitrogen gas. The soldering material was pure indium for most of the samples. Only 15 samples were soldered with pure tin to study the influence of contact material.

Data on the important bulk electrical parameters of the six types of InSb crystals are listed in Table 1. Also given in the Table are the length ranges and the number of samples in each group.

2. Results

A schematic diagram of the experimental set-up is shown in Fig. 2. Here R_x is the variable resistance while the external resistance R_e is equal to the sum of R_x, R_I and the output resistance of the power supply. Six typical I-V curves representing six groups of different samples with indium contacts are shown in Figure 3

through 8 while Fig. 9 shows the influence of using tin as contact material. Because six kinds of InSb and two kinds of soldering materials were used, these I-V curves are different from one another. However, regardless of what kind of InSb or solder is used, they all have a branch of negative differential resistance (NDR). In general, two basic shapes are found for samples with pure indium solder. They are: (1) a linear relationship between current and voltage in the low current range, then a constant current line, and then an NDR branch, and (2) a bent curve starting from the origin followed by an NDR branch. For samples with pure tin solder, the I-V curves are not consistent enough to be described in general terms, especially for the PH and PM groups. However, all n-type group samples with tin solder start with a linear segment in their I-V curves, as exemplified by the curve of Fig. 9 for a sample form the NL group with tin contacts.

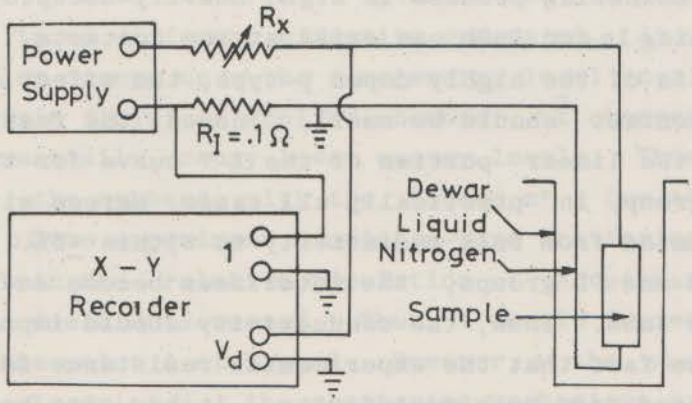

Fig. 2. Experimental setup for quasi-static investigation.

3. Discussion of Results

In this section, the linear segment, the jumps, and the constant current line are discussed. The NDR branch (due to avalanche breakdown) and a bent I-V curve at low currents (due to p-n junction formation at the contacts) are related to the theory to be developed in Section III and will therefore be discussed later.

(1) Linear Segment

As can be seen from Figures 3 through 5, p-type samples using indium solder have straight I-V curves at low currents. On the other

hand, for tin solder, this portion of the I-V characteristics may be straight (see, e.g., Fig. 9) or bent, depending on the carrier concentration involved. These observations indicate that the contact material has a strong influence on the transport characteristics of InSb at low voltages.

If the influence of surface states due to termination of the lattice and the existence of oxidation and impurities at the surface can be neglected, whether a metal-semiconductor contact is ohmic or rectifying depends in principle only on the relative values of the work function of the metal and semiconductor in question. However, due to the high density of surface states, the rectifying properties of metal-semiconductor junctions are usually independent of the values of the work functions. In the case of InSb with indium or tin solder, the situation is even more complicated.

Indium has three valence electrons and therefore can be considered as a p-type material relative to InSb. Since the temperature in the soldering process is high, heavily-acceptor alloyed region containing In and InSb can exist at the contacts. Thus, if the InSb sample is of the highly doped p-type, the effect of the resulting ohmic contact should be small. Indeed, the resistance calculated from the linear portion of the I-V curve for the 49 samples in the PH group, in practically all cases, agrees with the resistance calculated from bulk resistivity to within $\pm 5\%$.

For PM and PL groups, the interfaces become sources of holes to the bulk InSb. Thus, the conductivity should improve as demonstrated by the fact that the experimental resistance is smaller than that calculated from bulk resistivity. It has also been noted that as the sample length increases, these two resistance values are closer to each other, as the contact effect becomes less and less important with increasing sample length. For n-type samples the interface is a junction, and the associated phenomenon will be discussed in the next section.

Tin has four valence electrons. It is a neutral impurity relative to InSb. A comparison of measured resistance and calculated resistance shows that pure tin solder gives samples of both carrier type a barrier, especially for the NH group. In the latter case, the barrier resistance is much larger than the bulk resistance. For the PL group, the curves are bent and the calculated resistances are very large and it is difficult to see the contact effect. For the

remaining groups, the barriers are not high and straight I-V lines result.

(2) Jumps A-A', B-B' and H-H'

The A-A', B-B' and H-H' lines represent unstable paths and there are no stable points on them. In addition, the jump points are very much dependent on external resistance as discussed in Section I. Indeed, in every case, it can be easily verified that the slope of these lines is equal to $-1/R_e$ where R_e is the external resistance. Also, as anticipated from our discussion in Section I, there is hysteresis associated with these jumps; the size of the loop depends again on R_e.

A number of explanations can be advanced for this jump phenomenon. One plausible explanation is based on intra-band transitions. According to Fig. 6 of the forthcoming paper by Chelikowsky, Chadi, and Cohen, the valence band edge at $\vec{k}=0$ is two-fold degenerate when spin-orbit coupling is included. [11] When $\vec{k}$ departs from the (000) point, however, three different $\partial^2 E/\partial k^2$ values are possible. This gives rise to three different effective masses m*. At zero electric field, the holes occupy up to the same energy level in all subbands. When an electric field is applied, however, $\vec{k}$ changes and holes tend to preferentially occupy lower energy levels. This effect is strongest for the subband with the lowest m*. Due to the quasi-static nature of the experiment, the intra-band scattering mechanisms tend to maintain the relative population of the subbands constant as the electric field is increased. Thus, I should increase linearly with V_d up to the point A of Fig. 1. However, at the electric field corresponding to point A, the scattering mechanisms are no longer able to maintain the relative population of the subbands and an abrupt transition of holes from the band with the lowest m* to the one with next highest m* occurs, giving rise to a sudden decrease in the current at A, as observed within the limits of resolution of our experiment.

(3) Constant Current Line A-B'

If the electric field is increased further, the current is observed to stay constant, independent of V_d. This can be explained by noting that for the doping level considered, the relative population of the two bands can change in such a way, via bilateral scattering, as to maintain the total current constant irrespective of electric field.

The explanation advanced above should be most noticeable for PH group samples, as observed. Furthermore, V_A should decrease with increasing concentration, also consistent with experiment (see Fig. 10). For three of the PH group samples, a second abrupt drop in I occurs between V_A and V_B, presumably indicating a transfer of holes to the subband with the highest m*. If V_A is larger than the voltage required for avalanche breakdown, no abrupt change in I occurs as is the case for samples in the PL group.

No similar degeneracies occur at the conduction band edge and the separation between energy minima is too large to allow Gunn type transitions. Therefore, we expect no abrupt change in I for n-type samples with indium contacts, as observed.

(4) Avalanche Breakdown

When the sample voltage reaches the value V_B, the electric field at the contact regions may be quite large in the vicinity of surface imperfections. If its value is sufficiently high (note that 1V across 100 Å gives an electric field of 10^6 v/cm!), carries emerging from this region can have sufficient velocity to cause cumulative election hole pair creation and associated avalanche breakdown. This phenomenon is further studied in the next section.

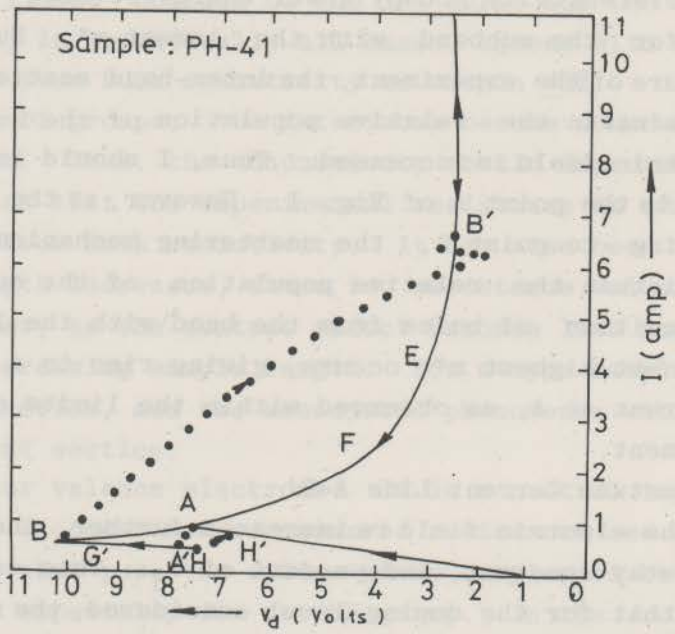

Fig. 3. Quasi static characteristics of InSb measured with various R: O-A-A'-B-B'-C, 2Ω; C-D, R_e=1Ω; B'-E, R_e=2Ω; E-F, R_e=5Ω and F-G'-H-H'-O, 10Ω.

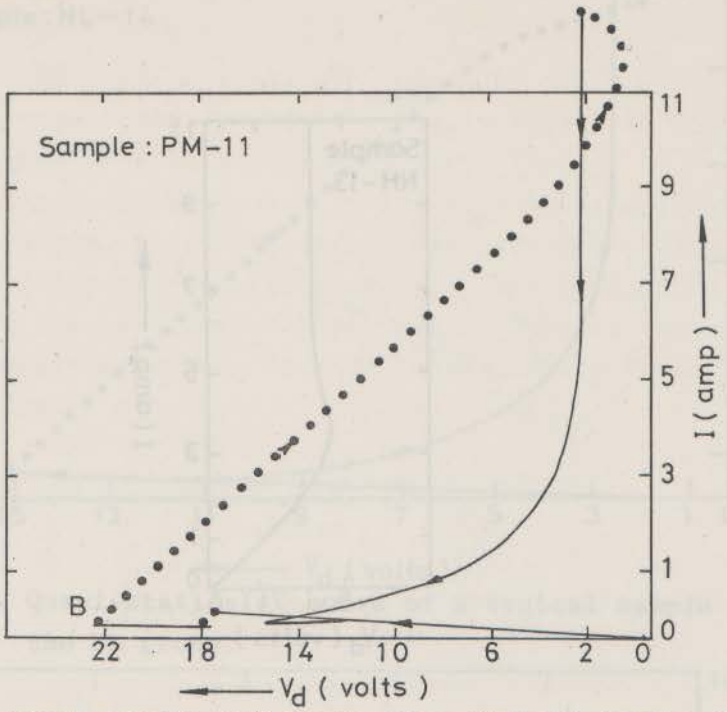

Fig. 4. Quasi-static I-V curve of a typical sample from the PM grom.

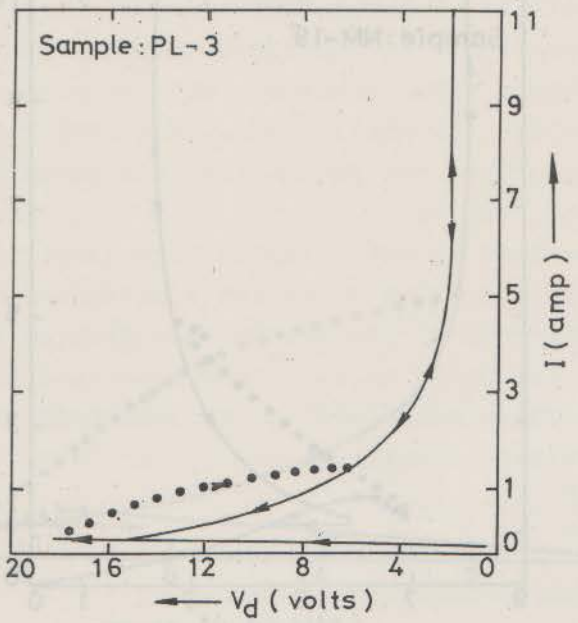

Fig. 5. Quasi-static I-V curve of a typical sample from the PL group.

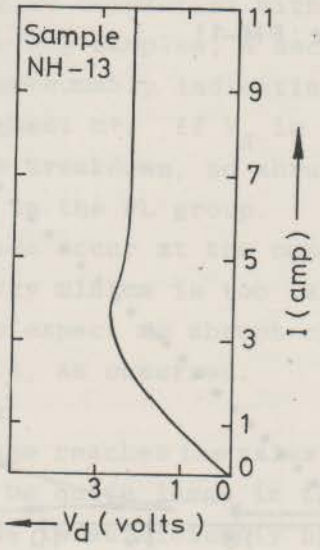

Fig. 6. Quasi-static I-V curve of a typical sample from the NH group.

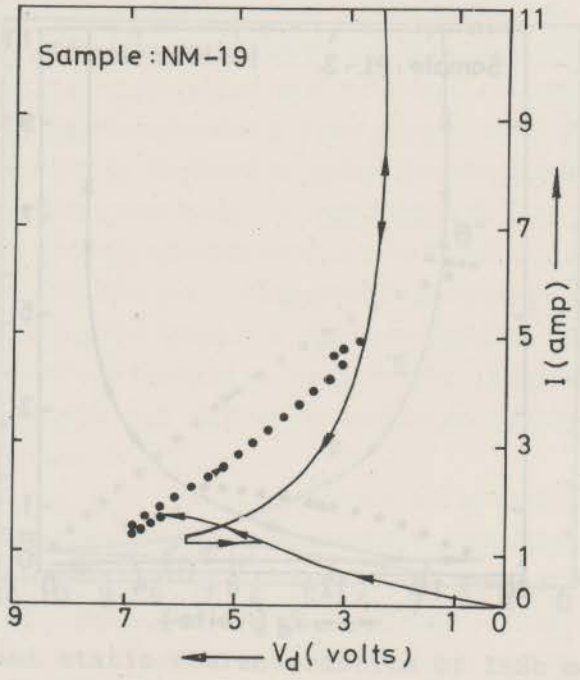

Fig. 7. Quasi-static I-V curve of a typical sample from the NM group.

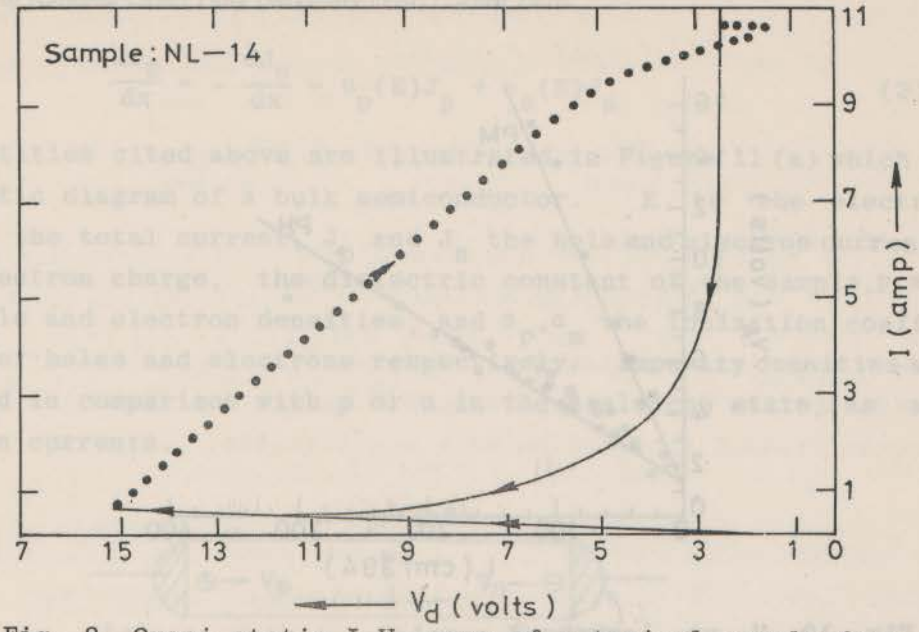

Fig. 8. Quasi-static I-V curve of a typical sample from the NL group.

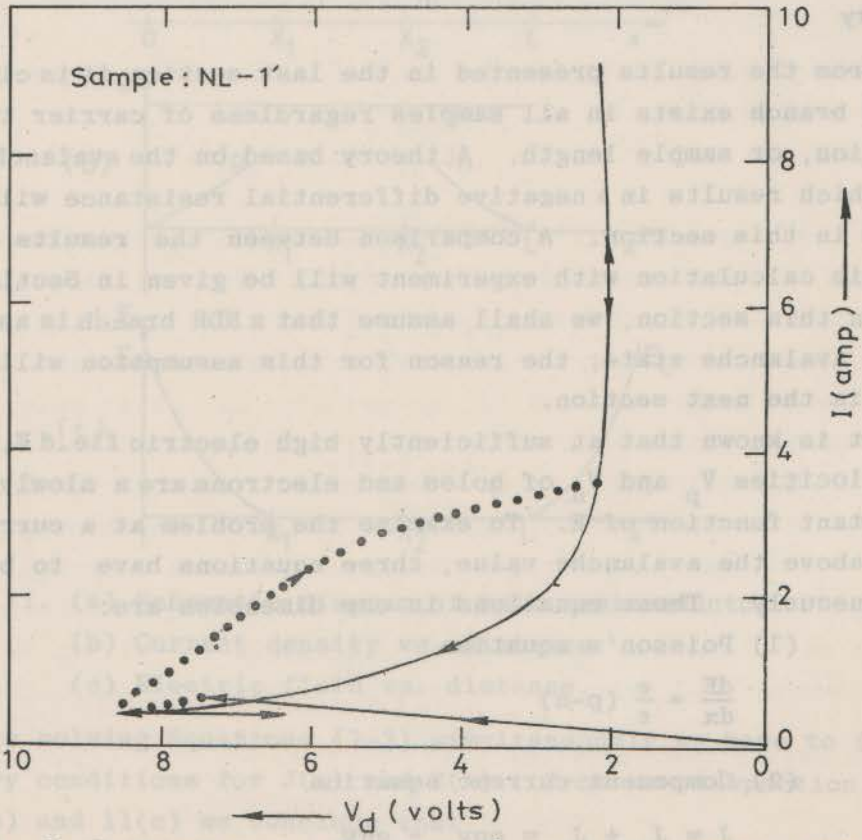

Fig. 9. Quasi-static I-V curve of a typical sample from the NL group with tin as contact material.

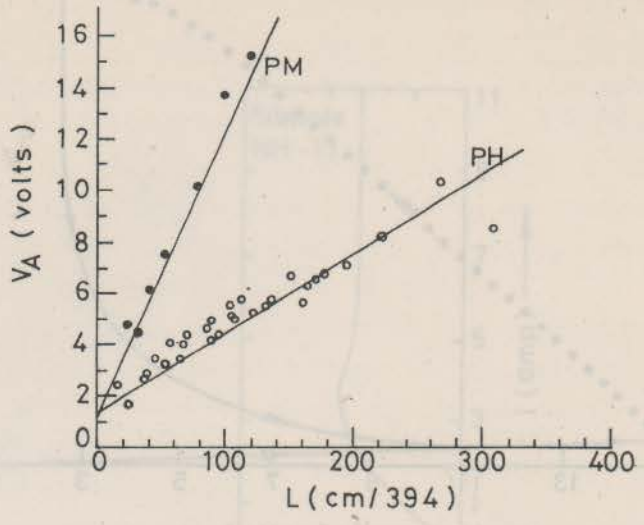

Fig. 10. V_A vs. length of sample.

III. Theory

From the results presented in the last section, it is clear that the NDR branch exists in all samples regardless of carrier type, concentration, or sample length. A theory based on the avalanche phenomenon which results in a negative differential resistance will be developed in this section. A comparison between the results obtained from this calculation with experiment will be given in Section IV.

In this section, we shall assume that a NDR branch is associated with an avalanche state; the reason for this assumption will be apparent in the next section.

It is known that at sufficiently high electric field E, the carrier velocities V_p and V_n of holes and electrons are a slowly varying or constant function of E. To examine the problem at a current density J above the avalanche value, three equations have to be solved simultaneously. These equations in one dimension are:

(1) Poisson's equation

$$\frac{dE}{dx} = \frac{e}{\varepsilon}(p-n) \qquad (1)$$

(2) Component current equation

$$J = J_p + J_n = epv_p + env_n \qquad (2)$$

(3) Carrier generation rate equation

$$\frac{dJ_p}{dx} = -\frac{dJ_n}{dx} = \alpha_p(E)J_p + \alpha_n(E)J_n \qquad (3)$$

The quantities cited above are illustrated in Figure 11 (a) which is a schematic diagram of a bulk semiconductor. E is the electric field, J the total current, J_p and J_n the hole and electron currents, e the electron charge, the dielectric constant of the sample, p and n the hole and electron densities, and α_p, α_n the ionization coefficients for holes and electrons respectively. Impurity densities are neglected in comparison with p or n in the avalanche state, as are diffusion currents.

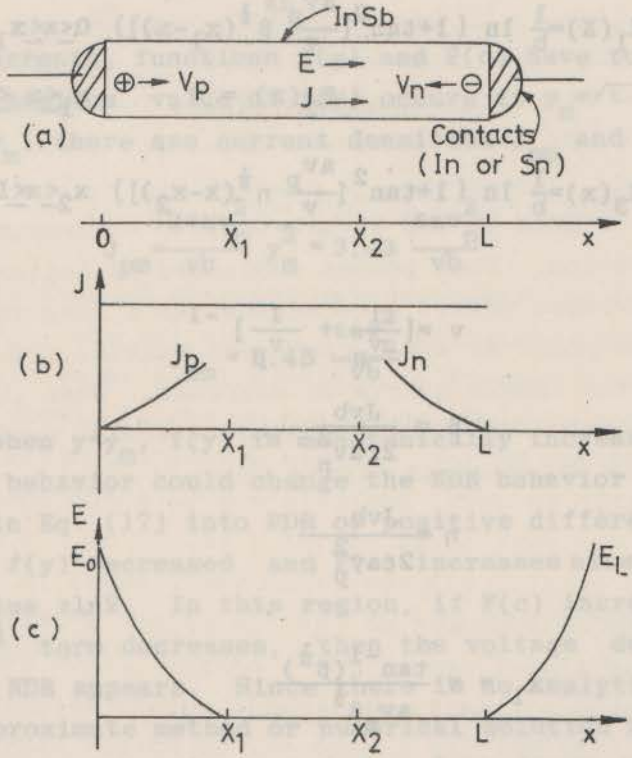

Fig. 11. (a) Schematic diagram of bulk semiconductor.
(b) Current density vs. distance.
(c) Electric field vs. distance.

Before solving Equations (1-3) simultaneously, we have to find the boundary conditions for J(x) and E(x). From an inspection of Figure 11(b) and 11(c) we conclude that

$$J(0) \simeq J_n(0) = ev_n\, n(0) \qquad \text{at } x=0 \qquad (4)$$

$$J(L) \simeq J_p(L) = ev_p p(L) \qquad \text{at } x=L \tag{5}$$

$$E(x_1) \simeq 0 \qquad \text{at } x=x_1 \tag{6}$$

and

$$E(x_2) \simeq 0 \qquad \text{at } x=x_2 \tag{7}$$

Now, if we assume that:

$$\alpha_p(E) = \alpha_n(E) = \alpha(E) = ae^{bE} \tag{8}$$

where a and b are constants (the exponential dependence of α is in accordance with McKay's experiments[12] on Si), we can solve for the electric field E as function of x analytically, i.e.,

$$E_1(X)=\frac{1}{b} \ln \{1+\tan^2[\frac{av_n}{v} \beta^{\frac{1}{2}}(x_1-x)]\} \quad 0\leq x\leq x_1 \tag{9a}$$

$$E_2(x) = 0 \qquad x_1\leq x \leq x_2 \tag{9b}$$

$$E_3(x)=\frac{1}{b} \ln \{1+\tan^2 [\frac{av_p}{v} \eta^{\frac{1}{2}}(x-x_2)]\} \quad x_2\leq x\leq L \tag{9c}$$

where

$$v =[\frac{1}{v_n} + \frac{1}{v_p}]^{-1} \tag{10}$$

$$\beta = \frac{Jvb}{2\varepsilon av_n^2} \tag{11}$$

$$\eta =\frac{Jvb}{2\varepsilon av_p^2} \tag{12}$$

$$x_1 = v \frac{\tan^{-1}(\beta^{\frac{1}{2}})}{av_n\beta^{\frac{1}{2}}} \tag{13}$$

and

$$x_2 = L-v \frac{\tan^{-1}(\eta^{\frac{1}{2}})}{av_p\eta^{\frac{1}{2}}} \tag{14}$$

If we define two functions f(y) and F(c) as:

$$f(y) = \frac{\ln(1 + y^2)}{1 + y^2} \tag{15}$$

$$F(c) = \int_0^c f(y)dy \tag{16}$$

Then the total voltage across the sample willl be given by:

$$-V=\int_0^L E(X)dx=\left(\frac{2\varepsilon\upsilon}{ab^3}\right)^{\frac{1}{2}}J^{-\frac{1}{2}}\left[F\left(\frac{Jvb}{2\varepsilon a v_n^2}\right)^{\frac{1}{2}}+F\left(\frac{Jvb}{2\varepsilon a v_p^2}\right)^{\frac{1}{2}}\right] \tag{17}$$

This is a nonlinear relation between current and voltage and in the above equation the factor $J^{-\frac{1}{2}}$ by itself will give an NDR curve. In fact, $F(\infty)$ has a definite value[13] $\pi\ln 2$. Thus, for very large currents, i.e., for very large $\beta^{\frac{1}{2}}$ and $\eta^{\frac{1}{2}}$, Eq. (17) becomes

$$-V=2\pi\ln 2\left(\frac{2\varepsilon\upsilon}{ab^3}\right)^{\frac{1}{2}}J^{-\frac{1}{2}} \quad \text{for } J\gg 1 \tag{18}$$

For small currents, functions f(y) and F(c) have to be further examined. The maximum value of f(y) occurs at $y_m=\sqrt{\varepsilon-1}\simeq 1.31$. Corresponding to y_m, there are current densities J_{pm} and J_{nm} given by:

$$J_{pm}=\frac{2\varepsilon a v_p^2}{vb}y_m^2\simeq 3.43\frac{\varepsilon a v_p^2}{vb} \tag{19a}$$

and

$$J_{nm}\simeq 3.43\frac{\varepsilon a v_n^2}{vb} \tag{19b}$$

Therefore, when $y<y_m$, f(y) is monotonically increasing and so is F(c). This behavior could change the NDR behavior due to the $J^{-\frac{1}{2}}$ term alone in Eq. (17) into PDR or positive differential resistance. For $y > y_m$, f(y) decreased and F(c) increases slowly and approaches a finite value $\pi\ln 2$. In this region, if F(c) increases less slowly than the $J^{-\frac{1}{2}}$ term decreases, then the voltage decreases as J increases and NDR appears. Since there is no analytical solution for F(c), an approximate method or numerical solution had to be exployed. The important conclusions drawn from these results are: (1) the I-V curve is nonlinear with PDR in the lower current region, but with an NDR in the higher current region, and (2) in the analysis of experimental results, it was found that I-V ourves can be represented by the empirical relation:

$$-V=(\text{constant})I^m \tag{20}$$

where I is current in ampere provided that m is 0.5 in the PDR region, and from less than -0.5 to -0.5, dependent upon current value, in the NDR region. This is in reasonable agreement with Eq. (17)

Furthermore, a numerical solution of (17) using a computer yields curves quite similar to those observed.

IV. Discussion

As we can see from Figures 3 through 8, regardless of the differences in the I-V curves at low-voltage-and-low-current range, all samples have an NDR branch. In fact, I-V curves of all 158 samples have this branch. We surmise from this that NDR in all samples may be due to some common basic mechanism.

From the discussion above, it is seen that the experimental results match very well with theoretical predictions. In order to check the theory itself, it is desirable to measure the field variation in the sample with increasing current. However, this task is quite difficult. Since the sample is bathed in liquid nitrogen, it is impossible to use those advanced potential probe techniques to monitor the field. Therefore, a conventional voltage measurement method is used. Figure 12 and 13 are results of measurement of the voltage distribution. Four probes indicated by letters W, X, Y, Z (O to be the reference point) are mounted on a long sample PH-49. At point B, the point at which avalanche starts, the field in the central part of the sample starts to decrease. When the current is larger than 1 ampere, the central field is almost zero, consistent with the situation depicted in Figure 11(c).

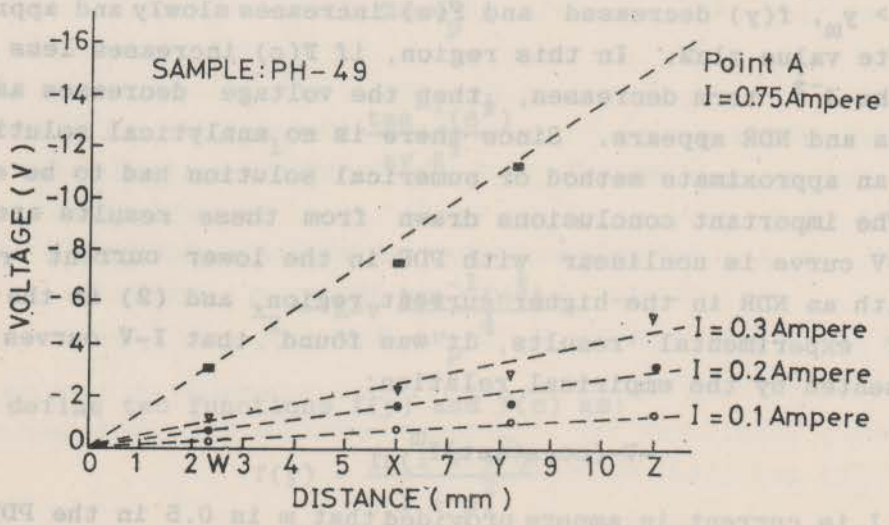

Fig. 12. Voltage distribution before abalanche.

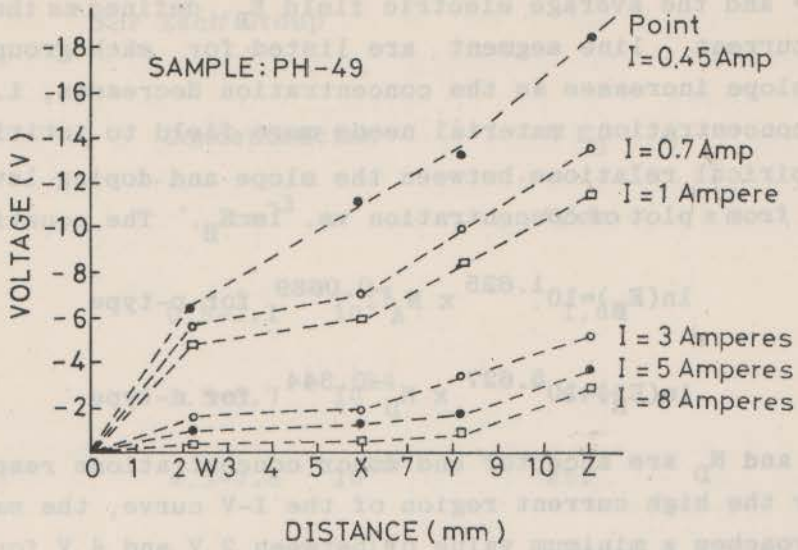

Fig. 13. Voltage distribution after avalanche.

It is also of interest to investigate the sample length dependence of V_B, the voltage at which avalanche begins; V_B corresponds to the voltage at point B marked in Figures 3 throgh 8. The plot of V_B vs. sample length for n-type groups have more linear relationship than any of the p-type groups. For PH and PM groups the curves can be approximated by two straight lines of different slopes, the line for $L < 3$ mm having a larger slope than the one for $L > 3$ mm. Also none of these lines intercept the voltage axis at zero. This indicates that a finite voltage is required to maintain avalanching even at very small lengths. The linear relationship between V_B and L for all samples at low I indicates that the average electric field E_B in the bulk region of the sample for the initiation of avalanche is independent of L. We should keep in mind, however, that the electric field distribution in the avalanche state, as sketched in F.g. 11(c), is far from being uniform. About all that can be said is that the voltage V_B minus the volatage at interface regions in directly proportional to the sample length. In Table 2, the voltage

---

* The voltage drop due to the solder contacts and cables at this low current is estimated to be about 0.17V which is small compared to the voltage drop across the sample.

as L → O* and the average electric field E_B, defined as the slope of the low current line segment are listed for each group. We note that the slope increases as the concentration decreases, i.e., lower carrier concentration material needs more field to intitial avalanche. Empirical relations between the slope and doping level can be obtained from a plot of concentration vs. ln E_B. The equations are:

$$\ln(E_B)=10^{1.625} \times N_A^{-0.0689} \quad \text{for p-type} \tag{21}$$

$$\ln(E_B)=10^{5.627} \times N_D^{-0.344} \quad \text{for n-type} \tag{22}$$

where N_A and N_D are acceptor and donor concentrations respectively.

For the high current region of the I-V curve, the sample voltage approaches a minimum value of between 2 V and 4 V for all samples, matching reasonable well with the voltages at zero length listed in Table 2. However, this measured voltage drop includes that due to solder contacts and cables which at high current levels can itself be of the same order and increases with increasing current.

Table 1. Parameters Of Samples

Group	Resistivity ohm-cm	Hall Coefficient cm^3-coulomb^{-1}	Hall Mobility cm^2-V^{-1}-sec^{-1}	Concentration cm^{-3}	No. of Samples In**	Sn**	Length Range mm
NB	0.0035-0.0050	3.0-7.0 10^2	0.85-1.4 10^4	0.90-2.1 10^{16}	14	3	0.881-4.60
NM	0.029 -0.0405	1.1-1.8 10^4	3.8 -4.4 10^5	3.5 -5.7 10^{14}	23	2	0.92 -12.97
NL	0.138 -0.270	0.8-1.4 10^5	5.2 -5.8 10^5	4.5 -7.8 10^{13}	19	3	0.587-12.67
PH	0.110 -0.125	4.7-5.2 10^2	4.2 -5.6 10^3	1.10-1.35 10^{16}	49	2	0.368-10.72
PM	1.07 -1.31	6.2-8.8 10^3	5.8 -6.7 10^3	0.7 -1.0 10^{15}	19	2	0.62 - 9.57
PL	23.0 -33.0	1.4-2.5 10^5	6.1 -7.6 10^3	2.5 -4.5 10^{13}	19	3	0.567- 9.93

* These data were evaluated at liquid nitrogen temperature (78°K) by Cominco American Incorporated: The resistivity by four-point probe at zero magnetic field; the Hall coefficient by two-point probe in a magnetic field of 1.6 KG.

** Materials used for making contacts.

Table 2. Voltage At Zero Length And Electric Field E_B For Each Group

Group	Concentration cm^{-3}	E_B V/cm	$V_{L=0}$ V
NH	$0.9\text{-}2.1\ 10^{16}$	1.64	2.02
NM	$3.5\text{-}5.7\ 10^{14}$	6.06	2.6
NL	$4.5\text{-}7.8\ 10^{13}$	25.	4.8
PH	$1.1\text{-}1.35\ 10^{16}$	26.8	1.53
PM	$0.7\text{-}1.0\ 10^{15}$	54.2	3.85
PL	$2.5\text{-}4.5\ 10^{13}$	132.3	2.7

V. Acknowledgment

The authors wish to thank Professor C.Y. Fong of the Physics Department at the University of California at Davis for discussions.

References

1. M. Toda, Japan J. Appl. Phys. 2, p. 776 (1963).
2. M. Glicksman: Plasma Effects in Solids, Dunod, Paris, 1965 p. 149.
3. R. D. Larrabee and W. A. Hicinbothem, Jr.: Plasma Effects in Solids Dunod, Paris, 1965, p. 181.
4. T. O. Poehler, J. R. Apel and A. K. Hochberg, Appl. Phys. Lett. 10, p. 244 (1967).
5. B. Ancker-Johnson: Semiconductors and Semimetals I, Academic Press, New York, N. Y., 1966 p. 379.
6. B. Ancker-Johnson, Proc. IX Int's. Conf. Phys. Semicon., Moscow, 1968, Nauka, Leningrad, 1968, p. 813.
7. A concise review of the subject has been given by M. Glicksman, IBM J. Res. Develop. 13, p. 626 (1969).
8. L. F. Eastman, Inst. Electrical Electronic Engrs. Trans. Electron Devices ED-

13, p. 117 (1966).

9. C. Tsai and R. F. Soohoo- Bull. Am. Phys. Soc. 14, p. 1159 (1969).
10. C. Tsai and R. F. Soohoo, Bull. Am. Phys. Soc. 18, p. 16 (1973).
11. J. Chelikowsky, D. J. Chadi and Marvin L. Cohen, Phys. Rev. (to be published). We thank J. Chadi for making this paper available to us before publication.
12. I. S. Gradsnteyn and I. M. Tyzhik: Table of Integrals, Series & Products, Academic Press, New York, 1965, p. 560.